

Near the jamming transition of elastic active cells: A sharp-interface approach

Yony Bresler, Benoit Palmieri, and Martin Grant*
Physics Department McGill University Montreal Canada
 (Dated: March 22, 2022)

We use a sharp interface model for active cells to study the jamming transition point and behavior near it by varying cell concentration, active velocity and elasticity, including a binary mixture of soft and stiff cells. We determine the jamming transition point, as well as behavior near the transition, including the effective diffusion, and sixfold bond correlations. Finally, we expand on previous studies by showing the Voronoi dimensionless cell shape can be treated as an order parameter at any concentration.

Usage Secondary publications and information retrieval purposes.

PACS numbers May be entered using the environment PACS numbers.

Assemblies of cells can behave as a liquid, or as a solid. Recently, the study of how biological processes relate to concepts such as jamming and the glass transition have gained attention. These studies include experiments, such as jamming during cancer invasion [13, 24], ongoing jamming in the corneal endothelium [8], self-driven jamming in microbial growth [10], and unjamming in wounds [9]. There have also been theoretical biophysics studies, which have established a connection between cell migration and glass dynamics [1], direct measurement of the transition with varying concentration for soft disks [15], and a proposed jamming phase diagram [30]. Notably, the Vertex [5] and Self-propelled Voronoi [6] models showed that cell shape can be used to determine the jamming state. These studies have also recently been extended to 3D [21].

Though driven and active system are far from equilibrium, they have been shown to share key features with the equilibrium glass transition, such as effective thermal behavior and time correlation functions [3, 4]. However, despite a wide range of experimental and theoretical work on the glass transition, several fundamental questions remain unanswered or contested [17, 26, 31]. In two dimensions, one must consider a potential Kosterlitz-Thouless-Halperin-Nelson-Young hexatic phase [16, 32]. Indeed, this has been seen, for example in colloidal films [27] and in repulsive Monte Carlo simulations [28], although for hard-core or very short-range interactions, transitions appear to be first-order [2]. Whatever the case may be for active systems, these results for thermal systems will play a role.

In this letter we wish to extend these studies using our recently developed model for elastic cells [7], a sharp interface limit of a phase field model of cells [25], which shares some similarities with the recently released *CellSim3D* model [18]. Points along a cell interface $\mathbf{R}(\theta)$, with elasticity γ evolve by minimizing the local curvature K , setting a preferred cell area πR_0^2 , in the presence of repulsion forces due to the other cells, and the cell velocity. More precisely, the time evolution for cell n is given in dimensionless units by

$$\partial_t \mathbf{R}_n(\theta, t) = \left[\gamma K(\theta, t) - \frac{1}{R_0} + \mu (A_n - \pi R_0^2) + \beta (\tanh(\alpha d_{n,\theta}) - 1)^2 \right] \mathbf{n}_\theta + \mathbf{v}_n, \quad (1)$$

where $K(\theta, t)$ is the local curvature of the interface, $\frac{1}{R_0}$ is the natural curvature of a spherical cell, μ sets the strength of the preferred cell area, A_n is the current area, λ is the interface thickness, $\alpha = \sqrt{\frac{15}{2}}/\lambda$, $\beta = \frac{150}{\alpha\lambda}$ and $d_{n,\theta}$ is the distance to the nearest neighboring cell along the local normal to the interface \mathbf{n}_θ . The cell velocity \mathbf{v}_n is the sum of active and inactive terms: The active velocity has a constant magnitude v_A , and reorients with probability $P(t) = \frac{1}{\tau} e^{-t/\tau}$, where τ is the mean time between reorientations. Inactive velocity is due to forces exerted by the other cells surrounding it as well as the substrate and surrounding water. The model can be used at any degree of confluence, or concentration, $\rho = \frac{N\pi R_0^2}{L^2}$, where N is the number of cells and L is the length of the simulation box. This does not take into account the distance between adjacent interfaces which is proportional to λ , and hence it under-represents slightly the actual degree of confluence. Cell stiffness was increased three-fold from our previous study, $\gamma = 1.35$ for 'soft' cells and $\gamma = 3.75$ for 'hard' cells, while v_A was varied throughout. The rest of the simulation parameters were unchanged, $\lambda = 7$, $R_0 = \lambda^2$, $\mu = 0.5$, $\tau = 10^4$, $\epsilon = 10^3$ and time integration step $dt = 0.1$, all given in a.u.. Each simulation consists of 288 cells in a square box with periodic boundary conditions. Simulations were run for at least $t = 800,000$ after an equilibration of $t = 80,000$ from an initial hexagonal configuration. We expect that our results extend beyond the exact details of the model as the long-time behavior has been shown to be independent of model details in a dense liquid near the glass transition [12].

We begin by demonstrating that our system can reach the jammed state. Under the right conditions, the active velocity is unable to allow a cell to squeeze through its neighbors leading to dynamical arrest. Fig. 1(a) shows a

arXiv:1807.10318v1 [cond-mat.soft] 26 Jul 2018

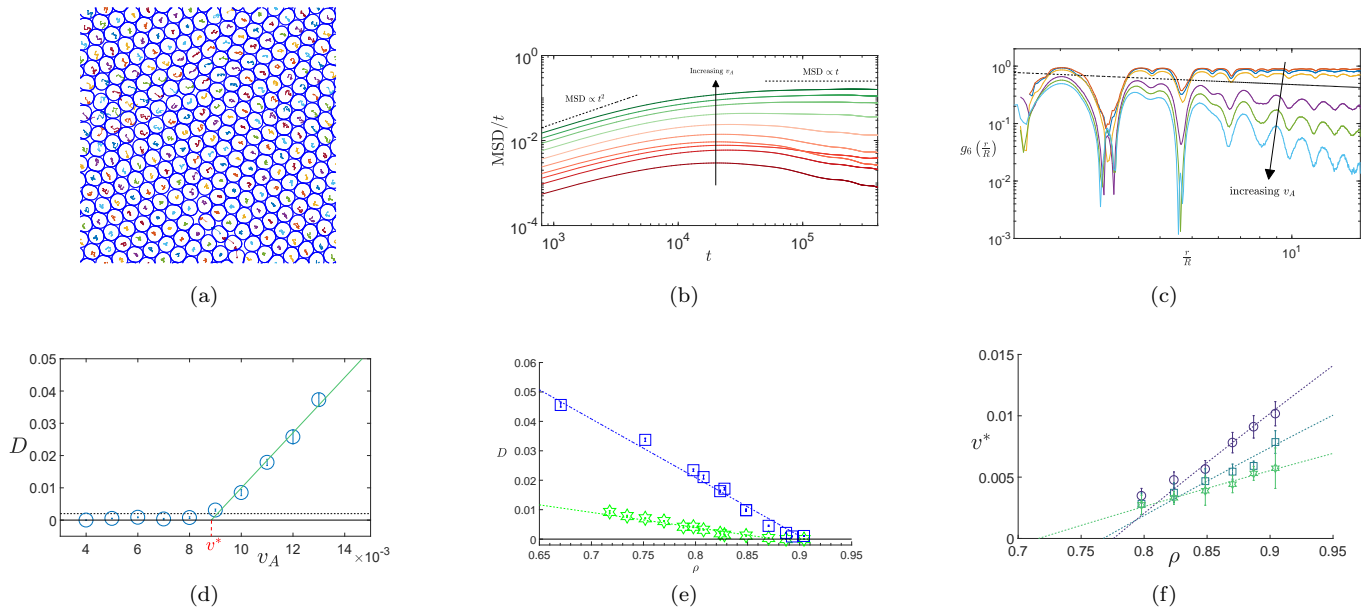


Figure 1: **Signatures of Jamming.** (a): snapshot of cell interface in jammed state, colored lines trace cell center of mass over $t = 8 \cdot 10^4$, (active velocity $v_A = 0.0075$, degree of confluence $\rho = 87\%$, all normal cells). (b): Mean square displacement over time for a range of increasing active velocities shows initial ballistic motion $t \ll \tau = 10^4$. Late times show jammed behavior becoming diffusive as v_A is increased ($\rho = 89\%$, all normal cells). (c): Sixfold Bond correlations, $g_6(r)$ for a series of simulations ($\rho = 87\%$, all normal cells) plotted on a log-log scale. The dashed line is a guide to the eye at the predicted KT algebraic decay $\eta = \frac{1}{4}$. (d): Effective diffusion constant decreases linearly with v_A before reaching a noise floor $2 \cdot 10^{-3}$ ($\rho = 89\%$, all normal cells). A best fit line (shown in green) is used to estimate the jamming velocity v^* (shown in red). (e): Diffusion with fixed v_A with varying concentration for two parameter sets: blue ($v_A = 0.006$, 50% mixing), and green ($v_A = 0.003$, 100% soft). Both are in good agreement with single-parameter fits (dashed lines) of Eq. 2. (f): Jamming transition velocity as a function of concentration. Transition is consistent with linear mixing. Fit lines are single parameter fits according to Eq. 3.

snapshot of cell interfaces and their center of mass movements over $t = 8 \cdot 10^4$, showing most cells do not exchange neighbors. Of course, that alone is not sufficient evidence of jamming. As our system is active rather than thermal, we can cross the jamming point by varying v_A , the active motor strength. Keeping other parameters constant, Fig. 1(b) depicts the mean square displacement (MSD) over time as a function of simulation time. For short times $t \ll \tau$, all simulations show ballistic diffusion where $MSD \propto v_A^2 t^2$. By $t \gg \tau$ however, the behavior depends on v_A . Large active velocity (shades of green) have the expected diffusive behavior, $MSD \propto t$, and the magnitude decreases with v_A . Eventually v_A drops below a threshold and MSD becomes sub-linear (shades of red) indicating possible dynamical arrest due to caging effects. A more direct signature of a transition from a liquid to a jammed state is in the falloff of the bond correlations of the sixfold orientation order parameter [14] $\Psi_6(\mathbf{r}) = \sum_{j,k} e^{6i\theta_{jk}}$, where the sum is over every neighbor k within $2.5R_0$ of cell j , and $\theta_{jk}(\mathbf{r})$ is the angle between them relative to the x -axis. A solid exhibits long range orientational order, and the bond-orientational correlation function $g_6(r) = \langle \psi_6(\mathbf{r}) \psi_6^*(\mathbf{0}) \rangle$ approaches a nonzero constant for large r , whereas in a liquid it decays

exponentially with a characteristic correlation length ξ , $g_6(r) \sim e^{-r/\xi}$. However, in between these may lie an additional hexatic phase, where bond orientation decays algebraically, $g_6(r) \propto r^{-\eta(T)}$. The Kosterlitz-Thouless theory also predicts the hexatic-liquid transition occurs when $\eta = \frac{1}{4}$ (and implicitly, the solid-hexatic transition is at $\eta = 0$) [20]. Figure 1(c) shows the bond orientational correlation function for a series of simulations. Low v_A are below the hexatic liquid transition shown as the dashed line. η grows with increasing motor strength, crossing into the liquid phase where the exponential fall-off would be faster than linear on this log-log plot. Given our system size, it is not possible to discern whether there exists an additional solid-hexatic phase transition.

We determine the transition point by examining the average effective self-diffusion constant, D , as a function of v_A in Fig. 1(d). It is computed using the Green-Kubo relation $D(t) = \frac{1}{2} \int_0^t \langle \mathbf{v}(t') \cdot \mathbf{v}(0) \rangle dt'$ and averaging over late times. We see D decrease linearly with v_A , until it vanishes below a noise floor of $D < 2 \cdot 10^{-3}$. Using a linear best fit we label the point at which diffusion vanishes as v^* . We will show that this coincides with other signatures of a jamming transition. See supplemental information for simulation videos below ($v_A = 0.008$), very near

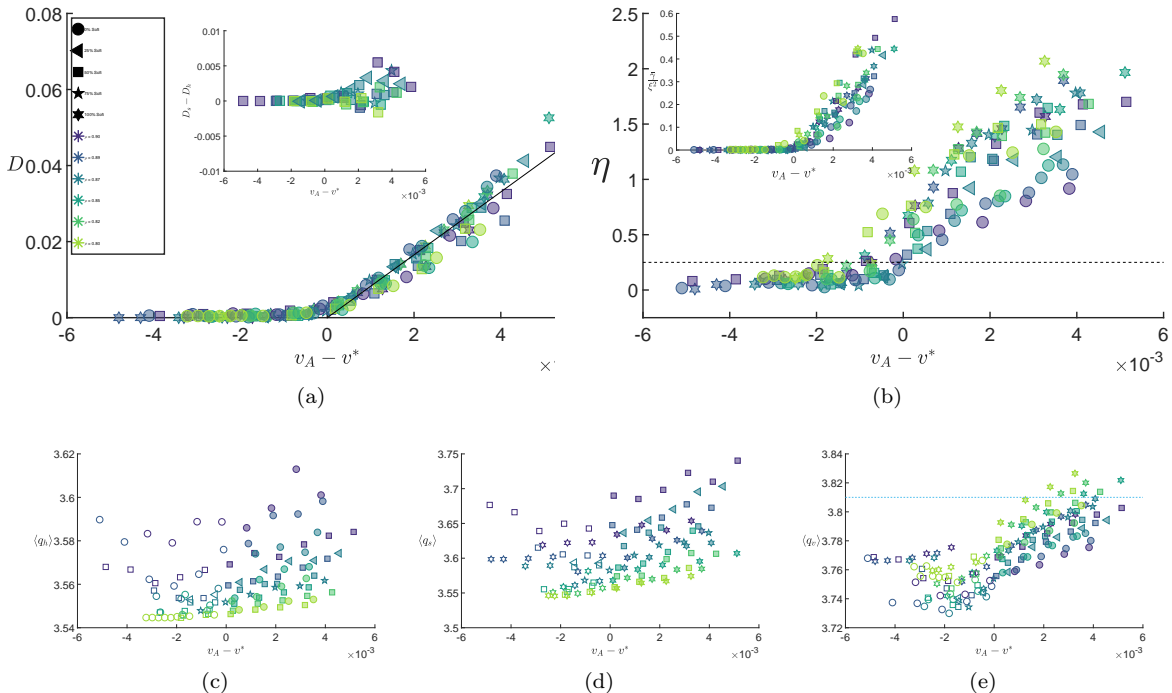


Figure 2: **Behavior across the jamming transition.** Symbol shape and color denote mixing ratio and concentration, respectively, as shown in legend top left. **(a):** The effective diffusion shows universal behavior above the jamming transition. Solid line is a single parameter line of best-fit. Inset: the difference between diffusion of soft and hard cells within the same simulation. **(b):** η (algebraic) fit to g_6 , consistent within error that the transition occurs at the value predicted from KT theory, $\eta = \frac{1}{4}$ (shown dashed line). Inset: Exponential correlation of the liquid state ξ appears linear and universal upon rescaling. Average dimensionless shape index for hard cells **(c)**, soft cells **(d)** and Voronoi tessellation **(e)**. For both soft and hard cells, shape index generally increases after unjamming, but transition value varies with simulation parameters. Using Cell center positions from our simulations, the Voronoi tessellation shows a more consistent value, though different from previous prediction $\langle q \rangle_{SPP} = 3.81$, shown as dashed line. For all 3 figures, results in the jammed regime are shown with unfilled symbols as they are sensitive to equilibration procedure.

($v_A = 0.009$) and above ($v_A = 0.010$) the jamming transition. Note these include the equilibration time, which is discarded from all statistics.

We use a similar idea to the Turnbull free volume model to obtain the effective diffusion for a thermal liquid near jamming [34]: consider a single cell with velocity v_A moving towards a fixed channel of width $d < 2R + \lambda$. For the cell to squeeze through, the dominant term of Eq. 1 that must be overcome is due to the curvature of the cell. Hence, there exists a minimum velocity needed to fit through, which is given by $v^* \propto \frac{\lambda}{d}$. If $v_A \leq v^*$, the cell will not be able to squeeze into the channel and become jammed. Higher motor velocities will be able to squeeze through and have net velocity $v_{eff} = v_A - v^*$, and indeed, we see this in simulations of an isolated cells and immovable square channel. Given this effective velocity, and that the system is still diffusive, we obtain $D \propto (v - v^*)$. As we will show, this model is also effective at predicting the transition velocity as well as diffusion in the dilute regime.

Another method for detecting the transition expands

on a result from our previous studies [7] by investigating the effective diffusion for a fixed v_A as concentration is varied. Fig. 1(e) shows the result remains linear, but now we must account for jamming, and

$$D(\rho) = \text{Max} \left\{ D_0 \left(1 - \frac{\rho}{\rho^*} \right), 0 \right\}, \quad (2)$$

where $D_0 = \frac{1}{2}v_A^2\tau$ is the diffusion of an isolated cell, and ρ^* is the concentration at which jamming occurs, i.e. $v_A = v^*$. The single parameter lines of best-fit show good agreement and suggest a method for estimating the onset of jamming purely from the diffusion of unjammed cells in a more dilute concentration. This differs from previous results of self-propelled soft disks [11], we expect due to details in the self-propulsion model.

We performed simulations over a range of concentrations (0.92% – 0.80%) and mixing ratios of soft to hard cells (0, 25, 50, 75 & 100%). For each parameter set, v_A was varied and a linear fit of $D(v_A)$ for values above the noise floor were used to estimate the transition point, where $D(v^*) = 0$. The results are summarized in Figure 1(f). Each series represents different mixing ratios

of soft and hard cells. As expected, both higher concentration and harder cells lead to transition at higher velocity. This reaffirms some of the known behavior of the jamming phase diagram [22]. Using the same simple model of the cell squeezing through a channel, and the free volume between adjacent hexagonal cells, we obtain

$$v^*(\rho) = \bar{\gamma} \frac{2 \cdot 3^{\frac{1}{4}}}{\sqrt{\pi}(R + \lambda/2)} (\sqrt{\rho} - \sqrt{\rho_J}), \quad (3)$$

where $\bar{\gamma}$ is the average elasticity of all cells, and ρ_J is the concentration of point J where jamming occurs at zero velocity. This single parameter fit is shown as a dashed line and is in good agreement with our results, particularly for the harder cells and mixed cells, and gives similar estimates for ρ_J . This is within error of previous results [22, 23] for soft repulsive discs, $\rho_J = 0.843$, since our definition of ρ does not include the interface width. The soft cells, as well as the results at the lowest concentration, appear to have larger systematic error, likely due to the smaller values of v^* approaching our noise floor.

Having determined v^* for each series, we now examine behavior across the jamming transition, $v_A - v^*$ in Fig. 2. In all plots, symbol color denotes concentration, while the symbol shape denotes hard to soft cell mixing ratio, as shown in the legend. Figure 2(a) shows a compilation for the effective diffusion constant. $D(v_A - v^*)$ increases with a universal slope above the transition, as seen by the line of best fit. Once again, this is consistent with the prediction of our cell squeezing model. Furthermore, the best-fit slope $D(v - v^*) = 8.264(v - v^*)$, is surprisingly close to half the Turnbull coefficient [33], $2R/6 \approx 16.33$. In the case where both soft and hard cells are present, the average value is shown. The inset shows the difference in diffusion constant between soft and normal cells of the same simulation, where the y-axis is 10 times smaller than the main figure in order to highlight the small differences. Although there might be a slight bias for softer cells to have higher diffusion than normal cells in the same simulation at large $v_A - v^*$, the cells appear to unjam simultaneously as there is no discernible difference near $v_A - v^* \approx 0$.

Fig. 2(b) shows a similar compilation for η . Here we find similar but non-universal scaling. Our results appear consistent with the KT prediction $\eta(v - v^* = 0) = \frac{1}{4}$, though due to systematic error in determining v^* and η , we can not concretely rule out other results such as $\eta = 0.385$ which has been suggested in other work [19]. As η is poorly defined in the liquid state, the inset shows that the above $v_A - v^*$ the liquid correlation length ξ combined with the average elasticity appears to be universal, as $\bar{\gamma}/\xi^2 \propto v_A - v^*$.

Bi *et al.* showed [6] that using a self-propelled Voronoi, the average dimensionless shape index, $\langle q \rangle = \langle P \rangle / \sqrt{\langle A \rangle}$ (where P is the cell perimeter) was a universal order parameter. They found that at and below the transition exists a universal value $\langle q \rangle_{SPP} = 3.81$, which increases

above the transition. We see that the same does not hold for this model. The two panels show the average cell shape for hard (Fig. 2(c)) and soft (Fig. 2(d)) cells. Results below the jamming transitions are sensitive to equilibration procedure hence they are shown with hollow symbols. The figures show that while the shape index is increasing above the transition, the value varies significantly between soft and hard cells, as well as with concentration and mixing ratio, and hence is not a unique order parameter.

Of course, the self-propelled Voronoi model differs from our sharp interface in several ways, most significantly simulations are always performed at full confluence $\rho = 1$, cells have limited deformation, and all cells had the same elasticity. We make a more direct comparison by computing the Voronoi tessellation of the cell center of mass from our simulation, similar to that used to analyze the local structure and statistics of experimental cell data [29]. As shown in Fig. 2(e), the Voronoi shape index does appear to be a good order parameter for the transition. But our value at the transition $q_V^* \approx 3.765$ is lower than the self-propelled Voronoi model value ($q_{SPP}^* \approx 3.81$, shown as dashed line). Note that for $v_A - v^* < 0$ the shape index appears to go below the value at the transition for some simulations, in contrast to the self-propelled Voronoi model. We suggest that although the Voronoi shape index may be a useful order parameter, the transition value appears to be model dependent, and hence may vary between cell lines as well.

In conclusion, we have demonstrated that our elastic cell model reproduces both liquid and hexatic phase. For each parameter set, we estimate the velocity at the onset of jamming v^* , and our results are consistent with the hallmarks of jamming. Using a simple free volume argument along with simulation results, we have also shown the following relations: an exact relation for the transition velocity, shown in Eq. 3. That the effective diffusion is zero in the hexatic phase and has universal linear behavior with increasing v_A , and that that diffusion for a fixed v_A below the jamming concentration depends on the jamming value. The hexatic-liquid transition appears consistent with KT theory $\eta = \frac{1}{4}$, and in the liquid phase $\bar{\gamma}/\xi^2 \propto v_A - v^*$. Finally, we showed the shape index q of the actual cells (q_S, q_H) at the transition varies with system parameters. Using the shape index of the Voronoi tessellation, the transition appears constant at all concentrations and mixing ratios, $q_V^* \approx 3.765$, though this is lower than the previously predicted universal value.

We gratefully acknowledged The Natural Sciences and Engineering Research Council of Canada and the *Fonds québécois de la recherche sur la nature et les technologies* for funding this research, as well as *Calcul Québec* and Compute Canada for providing computing facilities.

-
- * Electronic address: martin.grant@mcgill.ca
- [1] Angelini, T. E., Hannezo, E., Trepap, X., Marquez, M., Fredberg, J. J., and Weitz, D. A., Proceedings of the National Academy of Sciences **108**, 4714 (2011).
 - [2] Bernard, E. P. and Krauth, W., Physical Review Letters **107**, 1 (2011), arXiv:1102.4094 .
 - [3] Berthier, L. and Kurchan, J., Nature Physics **9**, 310 (2013), arXiv:1302.4868 .
 - [4] Berthier, L. and Tarjus, G., Physical Review Letters **103**, 23 (2009), arXiv:0907.2343 .
 - [5] Bi, D., Lopez, J. H., Schwarz, J. M., and Manning, M. L., Nature Physics **11**, 1074 (2014), arXiv:1409.0593 .
 - [6] Bi, D., Yang, X., Marchetti, M. C., and Manning, M. L., Physical Review X **6**, 1 (2016), arXiv:1509.06578 .
 - [7] Bresler, Y., Palmieri, B., and Grant, M., , 1 (2018), arXiv:cond-mat.soft/1807.07836 .
 - [8] Brookes, N. H., (2017).
 - [9] Chepizhko, O., Lionetti, M. C., Malinverno, C., Scita, G., Zapperi, S., and La Porta, C. A. M., (2018), arXiv:1802.07488 .
 - [10] Delarue, M., Hartung, J., Schreck, C., Gniewek, P., Hu, L., Herminghaus, S., and Hallatschek, O., Nature Physics **12**, 762 (2016).
 - [11] Fily, Y. and Marchetti, M. C., Physical Review Letters **108**, 1 (2012), arXiv:1201.4847 .
 - [12] Gleim, T., Kob, W., and Binder, K., Physical Review Letters **81**, 4404 (1998), arXiv:9805200 [cond-mat] .
 - [13] Haeger, A., Krause, M., Wolf, K., and Friedl, P., Biochimica et Biophysica Acta - General Subjects **1840**, 2386 (2014).
 - [14] Halperin, B. I. and Nelson, D. R., Physical Review Letters **41**, 121 (1978).
 - [15] Henkes, S., Fily, Y., and Marchetti, M. C., Physical Review E - Statistical, Nonlinear, and Soft Matter Physics **84**, 84 (2011), arXiv:1107.4072 .
 - [16] Kosterlitz, J. M. and Thouless, D. J., Journal of Physics C: Solid State Physics **6**, 1181 (1973).
 - [17] Langer, J. S., Reports on Progress in Physics **77** (2014), 10.1088/0034-4885/77/4/042501, arXiv:1308.6544 .
 - [18] Madhikar, P., Åström, J., Westerholm, J., and Karttunen, M., Computer Physics Communications (2018), 10.1016/j.cpc.2018.05.024.
 - [19] Mazars, M., Arxiv preprint , 14 (2013), arXiv:1301.1571 .
 - [20] Murray, C. A., in *Bond-Orientational Order in Condensed Matter Systems. Partially Ordered Systems.* Springer, New York, NY (1992) pp. 137–215.
 - [21] Nogucci, H., (2018), arXiv:1802.09149 .
 - [22] O'Hern, C. S., Silbert, L. E., Liu, A. J., and Nagel, S. R., Physical Review E **68**, 011306 (2003), arXiv:0304421v1 [arXiv:cond-mat] .
 - [23] Olsson, P. and Teitel, S., Physical Review E - Statistical, Nonlinear, and Soft Matter Physics **83**, 2 (2011), arXiv:1010.5885 .
 - [24] Oswald, L., Grosser, S., Smith, D. M., and Käs, J. A., Journal of Physics D: Applied Physics **50** (2017), 10.1088/1361-6463/aa8e83.
 - [25] Palmieri, B., Bresler, Y., Wirtz, D., and Grant, M., Scientific Reports **5**, 11745 (2015).
 - [26] Parisi, G. and Zamponi, F., Reviews of Modern Physics **82**, 789 (2010), arXiv:0802.2180 .
 - [27] Peng, Y., Wang, Z., Alsayed, A. M., Yodh, A. G., and Han, Y., Physical Review Letters **104**, 205703 (2010).
 - [28] Prestipino, S., Saija, F., and Giaquinta, P. V., Physical Review Letters **106**, 235701 (2011).
 - [29] Rieser, J. M., Goodrich, C. P., Liu, A. J., and Durian, D. J., Physical Review Letters **116**, 1 (2016), arXiv:1509.05496 .
 - [30] Sadati, M., Taheri Qazvini, N., Krishnan, R., Park, C. Y., and Fredberg, J. J., Differentiation **86**, 121 (2013), arXiv:NIHMS150003 .
 - [31] Sillescu, H., Journal of Non-Crystalline Solids **243**, 81 (1999).
 - [32] Steinhardt, P. J., Nelson, D. R., and Ronchetti, M., Physical Review B **28**, 784 (1983).
 - [33] Turnbull, D. and Cohen, M. H., The Journal of Chemical Physics **34**, 120 (1961), arXiv:arXiv:1011.1669v3 .
 - [34] Turnbull, D. and Cohen, M. H., The Journal of Chemical Physics **52**, 3038 (1970), arXiv:arXiv:1011.1669v3 .